Short Communication

Influence of Crevice Thickness on Corrosion Behavior of API X80 Steel under Disbonded Coating in Acid Soil Environment

Bo Zhao[1,3], Hongxia Wan[2], Yunyan Peng[1], Chao Liu[3], Jun Li[1,*], Binan Shou[1]

[1] Institute of Chemical Analysis, China Special Equipment Inspection and Research Institute, Beijing 100029, China.
[2] Beijing Key Laboratory of Failure, Corrosion and Protection of Oil/Gas Facility Materials, Department of Materials Science and Engineering, China University of Petroleum (Beijing), Beijing 102249, China.
[3] Key Laboratory for Corrosion and Protection (MOE), Institute for Advanced Materials and Technology, University of Science and Technology Beijing, 100083, China.
[*]E-mail: zhaobo19840626@163.com

In this study, an experimental device based on the disbonded coating model for the Yingtan simulated soil solution has been developed. The corrosion behavior of X80 steel was studied by anodic polarization, electrochemical impedance spectroscopy (EIS) and scanning electron microscopy (SEM).The observed findings showed that the anodic polarization demonstrated "passivation" behavior when the crevice thickness was about 35 μm. However, the anodic current density increased and anode active dissolution tendency was sobered to enhance with the thickness. The charge transfer resistance (Rt) achieved the minimum and maximum values at a thickness of 150 μm and 400 μm respectively. The corrosion effects was noted to be serious at a thickness of 150 μm, and the pitting appeared due to the enhanced amounts of O_2 and H^+ migrating in the disbonded area, which was consistent with the findings from EIS.

1. INTRODUCTION

The pipeline steel is vital for the petroleum, gas and coal transportation over long distances [1-2]. The pipeline steel is protected against corrosion by using the outer coatings. However, the coating loses adhesion in the process of transportation or mechanical damage as well as aging degradation. These phenomena make it inevitable to produce bubbles and warping defects on the coatings [3-7]. With the electrolyte infiltration and long-term chemical and electrochemical evolution, specific corrosion

processes take place in the disbonded area, and the environment of the trapped solution in the disbonded area significantly differs from the external soil [8-9]. In addition, it is difficult for the cathode current to reach the bottom of the peeled coating, thus, the metal surface does not benefit from the effective cathodic protection [10-13]. The pipeline steel in the disbonded area suffers more severe corrosion damage and may promote local corrosion, such as pitting corrosion, crevice corrosion and stress corrosion cracking (SCC) [14-17]. A number of studies on the local chemistry and corrosion behavior under disbonded coating have been reported [18-21]. Therefore, the corrosion of pipeline steel under the disbonded coating is a serious issue and has attracted extensive attention from the researchers.

So far, the reported studies have focused on the various factors influencing the corrosion under disbonded coating. Wu et al. [22-24] studied the local chemical-electrochemical reactions under the disbonded coating. It was reported that the open-circuit potential moved negatively under the coating, and the potential in the bottom region was the lowest. In addition, the oxygen concentration at the bottom of the disbonded coating significantly decreased, whereas the accumulation of Cl^- and H^+ at the bottom of the gap enhanced the sensitivity towards stress corrosion. Ma et al. [25-28] studied the corrosion behavior of the disbonded coating under cathodic protection (CP). Owing to the separation of anode and cathode reaction sites, the steel corrosion was observed to occur preferentially in the crevice, and the potential difference between the coating fracture site and crevice reduced the effectiveness of the cathodic protection process. In addition, the microbial corrosion in the disbonded areas has been extensively studied [29-32]. The microbial concentration and corrosion behavior at different positions in crevices have been observed to vary greatly. Owing to a large number of experimental studies dealing with the corrosion medium, cathodic protection potential and microorganisms, the corrosion theory under the disbonded coating has been developed accordingly.

However, there are limitations in the research achievements due to the reason that the corrosiveness of the trapped solution towards the metal has been largely focused on, while ignoring the crevice thickness, which is one of the most important factors leading to trapped solution formation and subsequent corrosion. In this study, the crack model with different thicknesses was designed to simulate the corrosion behavior. The polarization curves and electrochemical impedance spectroscopy were used to analyze the samples having different crevice thicknesses. The corrosion morphology was observed by SEM. Finally, the corrosion theory was analyzed with respect to the crevice thickness.

2. EXPERIMENTAL

2.1 Electrodes and test solution

Test specimen were cut from a sheet used to generate X80 steel pipes. Its chemical composition (mass fraction %) was C 0.036, Si 0.197, Mn 1.771, P 0.012, S 0.002, Cr 0.223, Ni 0.278, Cu 0.220, Al 0.021, Ti 0.019, Mo 0.184, V 0.001, Nb 0.110 and balance Fe. The electrochemical measurements were performed using a three-electrode cell, where X80 steel was used as the working electrode (WE), platinum as the counter electrode (CE) and a solid Ag/AgCl electrode as the reference electrode (RE). The three-electrodes were embedded in an epoxy resin module (Fig. 1(a)), leaving an exposed area of a square with dimensions 0.5 cm × 0.5 cm for the working electrode, a circle with diameter (ϕ) of 0.1 cm

for the reference electrode and a rectangle with dimensions 0.3 cm × 0.8 cm for the counter electrode. The working surface of the module was subsequently ground with 150, 240, 400, 600, 800 and 1000 grit emery papers, successively. Afterward, the specimens were burnished to be scratch free and specular, followed by cleaning with distilled water and acetone.

To prepare a laboratory simulated disbonded model, a plastic shim was adjusted to control the crevice width (δ, μm), as shown in Fig. 1(b). The cover plate was used to tune the crevice thickness.
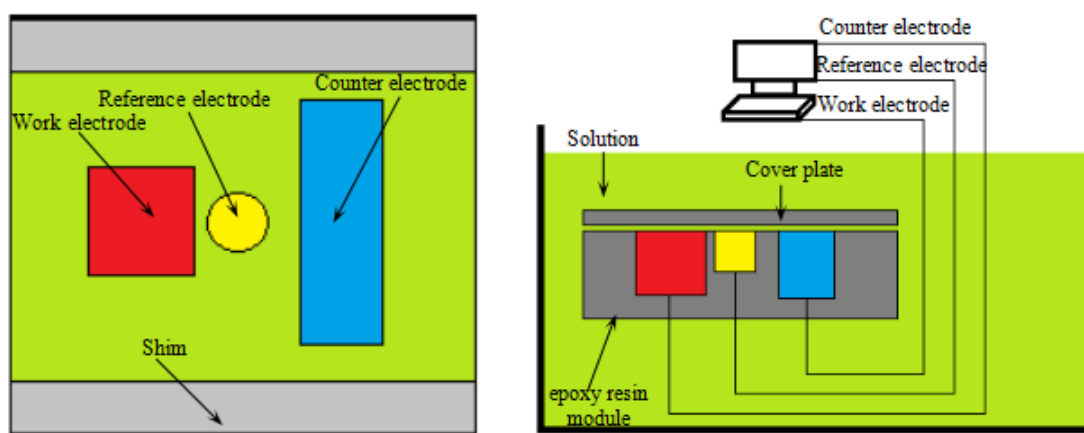

Figure 1. Test cell for the simulation of a crevice under disbonded coating.

The test used a type of solution simulate soil-extracted from Yingtan region in China, andthe chemical compositionsshowed in Tab.1. This was a kind of acid soil with pH of 4.5,and pH was adjusted by adding appropriate amount of 5% acetic acid.

Table 1. Chemical compositions of the simulated solution

pH	Chemical compositions　(mg/Kg)					
	NaCl	$CaCl_2$	KNO_3	$NaHCO_3$	Na_2SO_4	$MgCl_2 \cdot 6H_2O$
4.5	47.5	16.7	39.1	15.1	26.6	17.0

2.2 Electrochemical measurements

The electrochemical measurements were performed with a Princeton 2273 electrochemical system. The module was slowly immersed in the solution to ensure that the disbonded area was filled with the solution. The module was immersed for at least 30 min to ensure a steady state, which was identified by a stable corrosion potential. Subsequently, electrochemical impendence spectroscopy (EIS) and potentiodynamic polarization analyses were carried out. The test frequency range of EIS was 100 kHz~10 mHz, and the AC signal was 10 mV. Particular attention was needed while analyzing the potentiodynamic polarization as WE and CE were arranged together in the crevice, and the reaction occurring on CE might affect the chemical processes close to WE. This interference was significant in this study as the primary reaction product on CE was OH^-. As the test solution had a low pH of 4.5, the

generated OH⁻ significantly altered the local alkaline environment close to WE. Moreover, an enhancement in the distance between the WE and CE would raise the impedance on arranging the CE outside the crevice. Considering this, the potentiodynamic polarization analysis was contained in the anodic region. The anodic polarization curves were measured from the open circuit potential (OCP) to the positive direction until the potential reached 1V (vs. OCP) at a scanning rate of 1 mV/s. All tests were conducted at room temperature.

2.3 Analysis of corrosion products and morphology

The immersion test sample has dimensions of 10 mm × 15 mm × 2 mm, and three parallel samples were used. Prior to the analysis, the samples were ground to 120, 400, 800, 1200 and 1500 grit with silicon-carbide papers and subsequently mechanically polished with diamond polishing paste, followed by cleaning with anhydrous alcohol and drying. The immersion time for generating the corrosion layer was 10 days. In order to ensure the original state of the corrosion products, the experimental set-up was placed in deionized water with deoxygenation performed using N_2. After dehydration with anhydrous ethanol, the sample was swiftly dried and protected under N_2 until observation. The center of sample surface was selected as the observation position. The corrosion morphology and corrosion products were analyzed by scanning electron microscope (SEM, Quanta 250). In addition, the corrosion products were also analyzed by using energy dispersive X-ray spectroscopy (EDS). After characterizing the corrosion products, the samples were de-rusted using a descaling solution with 500 mL HCl, 500 mL H_2O and 3.5 g hexamethylenetetramine. After removing the corrosion products, the surface morphology of samples was observed by SEM. In order to indent the corrosion types, the cross-sectional images were processed by using a binarization method. The depth of the surface pits was measured using an optical focusing method.

3. RESULTS AND DISCUSSION

3.1 EIS and Polarization curve measurements

Fig. 2(a) shows the polarization curves and EIS of X80 steel in the simulated solution as a function of the disbonded thickness. A significant influence of the solution layer thickness was observed on the corrosion behavior of the steel substrate. The characteristics of the anodic polarization of X80 steel revealed some changes on reducing the thickness of the disbonded crevice. As the thickness of the crevice was 35 μm, the current density was constant when the potential was between 300 mV and 1200 mV which similar to the "passivation" phenomenon and the electrode reaction is inhibited. As the crevice thickness was enhanced o 70 μm, the "passivation" phenomenon was observed to be weakened. The anodic reaction exhibited a single activation system, however, the anode current density was increased with the crevice thickness.
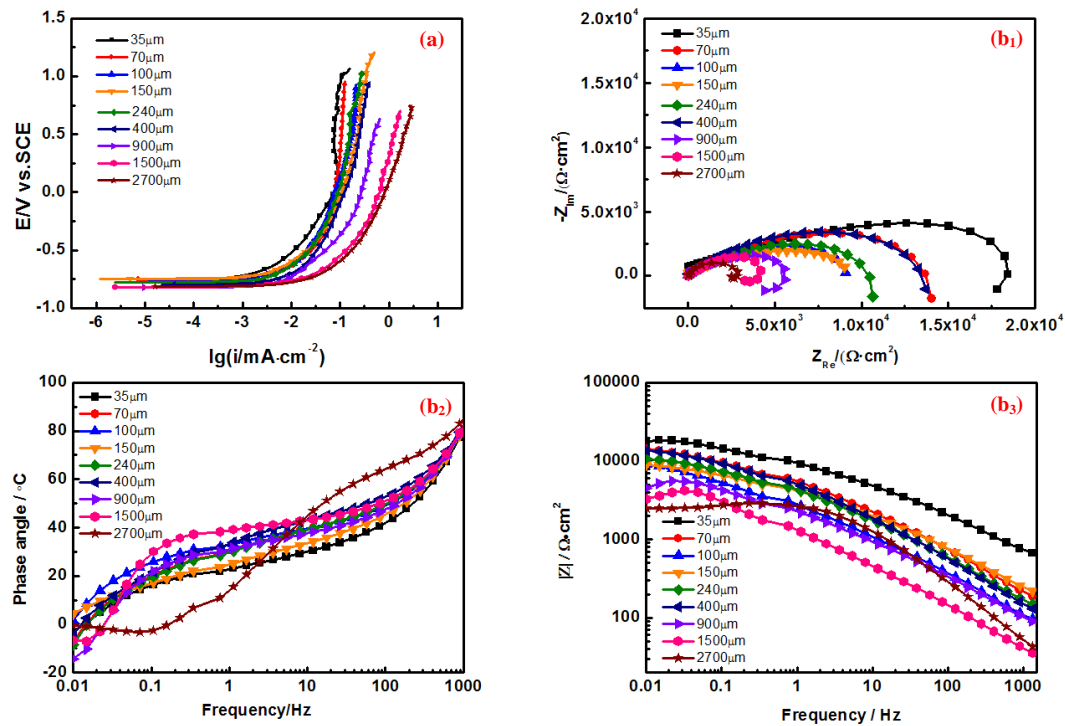
Figure 2. Electrochemical testing of X80 steel with different disbonded crevicethickness: (a) potentiodynamic polarization, (b$_1$) Nyquist of EIS, (b2)and(b3) Bode of EIS .

The reason for the observed phenomenon was the limited current diffusion on the electrode surface with thin crevice thickness in the disbonded system. Also, it could suppress the anodic reaction, thus, decreasing the corrosion rate. As shown in Fig .2(b1),(b2) and (b3), the EIS of X80 steel exhibited the similar characteristics for different crevice thicknesses, comprising of a high-frequency capacitive loop and a low-frequency inductive loop. The high frequency capacitive loop was related to the corrosion product on the electrode surface. Meanwhile, the low frequency inductive loop was related to the electrochemical reaction on the surface. To further analyze the impedance data, the impedance spectrum was fitted using ZSimpWin software. The impedance data could be fitted by the equivalent circuit containing two time constants, as shown in Fig.3.
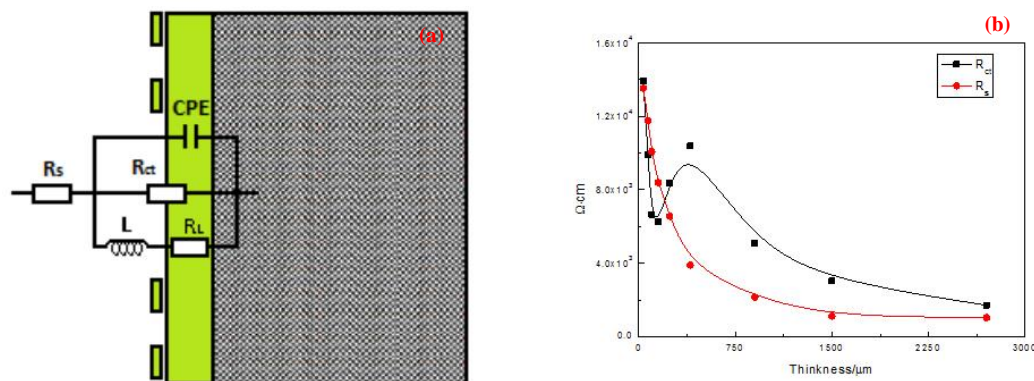

Figure 3. The fitting results of impedance data: (a)equivalent circuit, and (b) the R$_S$ and R$_t$ values with the crevice thickness change.

Fig. 3(a) shows the fitting equivalent circuit of EIS, where R_s represents the solution resistance, R_t is the charge transfer resistance and R_L is the inductive resistance. Fig. 3(b) shows the value of R_s and R_t as a function of the crevice thickness. As observed from Fig. 3(b), the R_s value decreased monotonically, which indicated that the mass transfer process during the electrode reaction was controlled by the thickness of the solution layer. It was observed to be consistent with the classical physics principles. The charge transfer resistance R_t was noted to increase regularly with the disbonded crevice thickness. The R_t value reaches the minimum when the crevice thickness was 150 μm, which showed the most serious at this crevice thickness. Subsequently, the Rt value increased with the disbonded crevice. When the thickness reached 400μm, the corrosion reaction was inhibited and the corrosion reaction was slow. Subsequently, Rt value continually decreased a steady state, when the crevice thickness is about 1500 um.
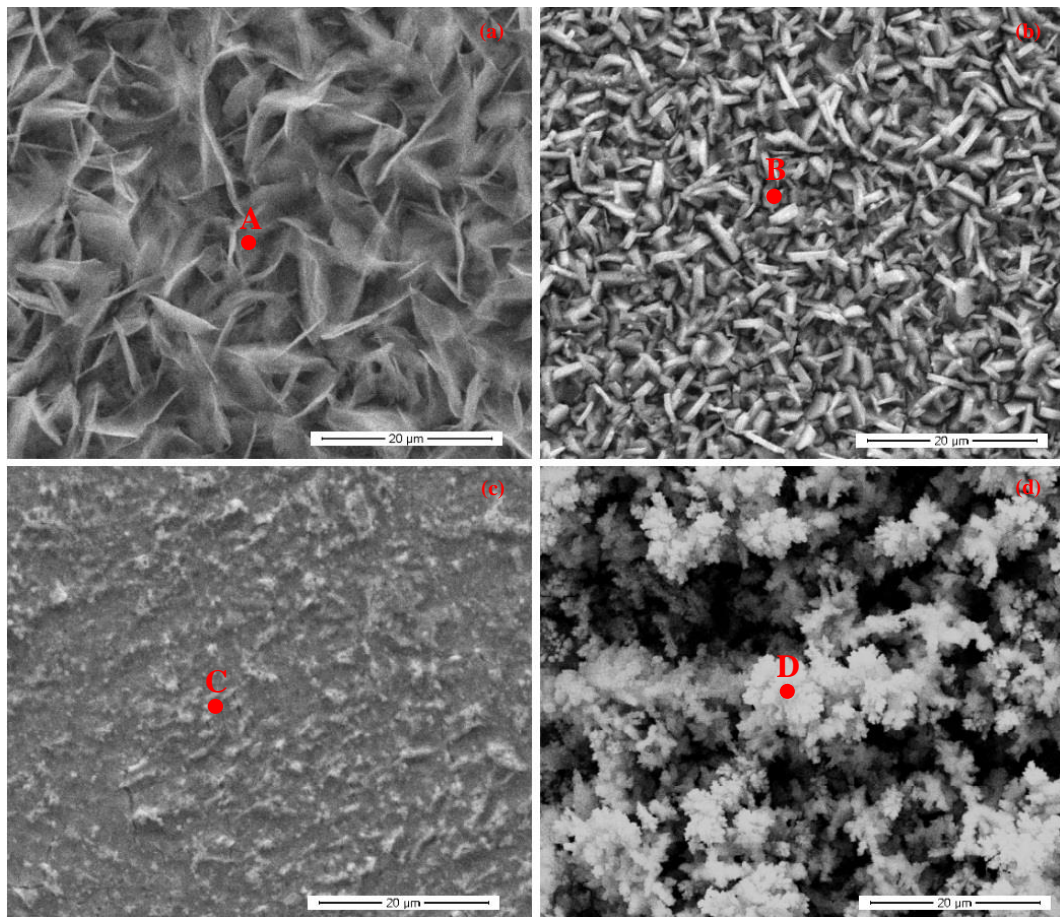

Figure 4. SEM images of X80 steel with corrosion products after immersion 10 days under different disbonded crevice thickness: (a) 35 μm, (b) 150 μm, (c) 400 μm and (d) 2700 μm.
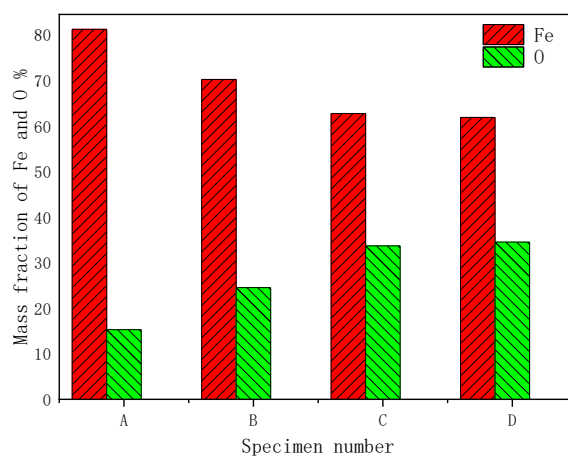
Figure 5. Mass fraction of Fe, O and C of corrosion products at A, B, C and D in Fig 4
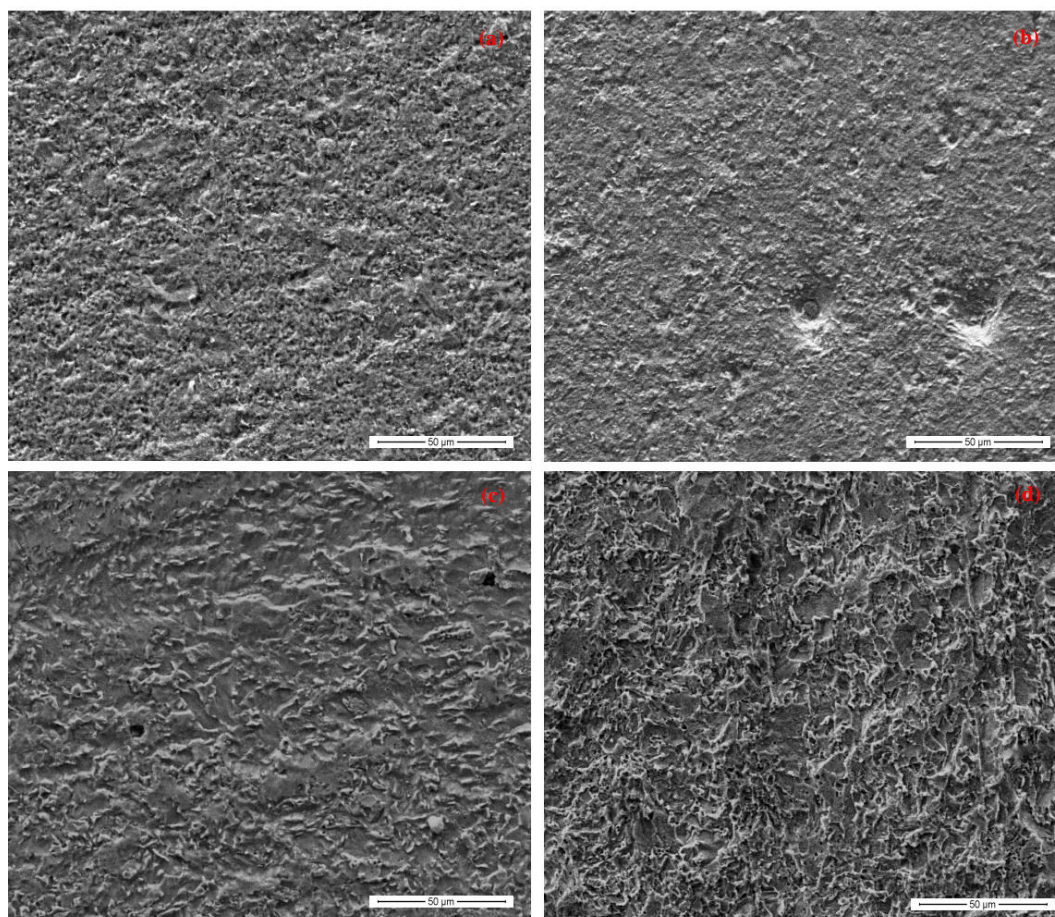

Figure 6. Morphology of X80 steel after removing the corrosion products after immersion for 10 days as a function of crevice thickness: (a) 35 μm, (b) 150 μm, (c) 400 μm and (d) 2700 μm.

Fig.4 shows the morphology of X80 steel with corrosion products and Fig.5 shows the EDS analysis of corrosion products of A, B, C and D 4-position. As can be noted, the corrosion products on

the four specimens showed extreme differences. When the crevice thickness is 35 μm, the corrosion products grow longitudinally to the larger size sheet. The products, with outer diameter of 15 μm, contained high Fe and low O contents, which indicated that the corrosion products were formed in the environment containing high Fe^{2+} concentration. As the disbonded crevice thickness was increased to 100 μm, the outer diameter of the corrosion products was reduced to 5 μm, and the thickness was enlarged, which exhibited a hexagonal prism structure. Compared with the case of 35 μm thickness, the Fe content was observed to decrease, while the O content increased in the corrosion products. For the disbonded crevice thickness increased to 400 μm, the corrosion products did not exhibit the typical geometrical configuration. This resulted in a protective effect on X80 steel due to the dense and effective coverage. Meanwhile, the Fe content decreased, whereas the O content was improved. As the thickness was further increased to 2700 μm, the corrosion products were of loose morphology, and the EDS analysis indicated that the Fe and O contents were consistent with the thickness of 400 μm.

Fig. 6 shows the morphology of the samples after removing the corrosion products. As can be observed, the general corrosion characteristics revealed insignificant corrosion at 35 μm crevice thickness. As the disbonded crevice thickness was increased to 150 μm, the surface of the specimens demonstrated the pitting morphology, and the pitting diameter was close to 20 μm, thus, indicating a high corrosion extent . As the disbonded crevice thickness was increased to 400 μm, the pitting diameter dropped down to 5 μm. Consequently, the corrosion characteristics were observed to revert to the general corrosion. As the disbonded crevice thickness was further increased to 2700 μm, the morphology presented the general corrosion character, however, the surface roughness was high, indicating severe corrosion.

3.3 Discussion

The R_{ct} variation could be divided into three stages (Fig.3). It was known that it existed two type of cathodic reactions of carbon steel corrosion in weak acidic solutions, which are hydrogen evolution and oxygen reaction, as the formula (1) and (2) showed[33]:

$$O_2 + 4H_2O + 4e^- \rightarrow 4OH^- \tag{1}$$
$$2H^+ + 2e^- \rightarrow H_2 \tag{2}$$
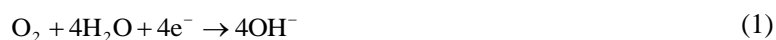
The anode reaction leads to Fe dissolution, as shown in (3):

$$Fe \rightarrow Fe^{2+} + 2e^- \tag{3}$$

For the disbonded crevice thickness of ≈35 μm, the crevice between the coating and substrate was small, and the trapped solution layer was thin, with a small amount of the electrolyte solution. The Fe^{2+} ions generated by the anode reaction were not able to diffuse and swiftly reached saturation in the disbonded area, thus, the anodic reaction was inhibited. On the other hand, the cathode electrode depolarization reaction is inhibited due to the rapid consumption of O_2 and H^+ as well as the crevice

occlusion effect. As the cathode and anodic reactions were inhibited, the corrosion reaction and corrosion rate were observed to slow down, which resulted in high reaction resistance and charge transfer resistance R_t. In this case, the morphology of the corrosion products appeared to acquire the sheet shape (Fig. 5(a)). This indicated that the corrosion products had high void fraction for the continuous growth of high concentrations of Fe^{2+} under the disbonded coating. At the same time, the morphology exhibited light corrosion after removing corrosion products due to the consumption of O_2 and H^+ in the solution layer under the disbonded coating (Fig. 6(a)). As the disbonded crevice thickness increased at the segment AB in Fig. 7 (35 μm < δ < 150 μm), the amount of the solution layer under the disbonded coating was also increased, with subsequent decrease in the Fe^{2+} concentration. Thus, the effect of Fe^{2+} on the electrode was weakened. Meanwhile, the ion diffusion channels were observed to be widened, which resulted in the weakening of the disbonded crevice occlusion effect. As cathodic reaction depolarization agents, the amount of O_2 and H^+ migrating into the disbonded area was enhanced. Different migration ability was observed for O_2 and H^+ due to the difference of concentration distribution under the disbonded coating. Specifically, the diffusion capacity of O_2 was poor, thus, the amount of O_2 migration into the disbonded area was less. The diffusion ability of H^+ was noted to be strong, thus, a larger amount of H^+ migrated into the disbonded area. Thus, H^+ ions swiftly entered the disbonded coating and gathered inside, which resulted in the trapped solution acidification [34-35]. Meanwhile, the Fe^{2+} ions hydrolyzed and generated more H^+, leading to the low pH of the trapped solution. It correspondingly enhanced the corrosiveness of the solution and decreased R_t to the minimum value. At point B in Fig. 7, the cathodic reactions at electrodes mainly performed the hydrogen evolution.

$$Fe^{2+} + 2H_2O \rightarrow Fe(OH)_2 + 2H^+ \tag{4}$$

According to Fig. 5(b), the corrosion products revealed a small circumscribed diameter, which is suggested to be $Fe(OH)_2$ formed through the hydrolysis reaction. After the removal of the corrosion products, 20 μm pitting was noted to appear, which was generated by the combined effect of the chemical and electrochemical reactions in the acidic solution system.

When the disbonded crevice thickness increasing between 150μm<δ<400μm. the amount of O_2 flowing into the crevice was enhanced, leading to strong oxygen reaction. The primary cathode reaction product was OH-, which enhanced the pH of solution in the crevice area. The hydrogen evolution reaction was noted to be suppressed, and the corrosion product changed to Fe_2O_3 at the same time. The reaction proceeded as the following equation:

$$Fe + Fe(OH)_2 + OH^- \rightarrow Fe_2O_3 + e^- \tag{5}$$
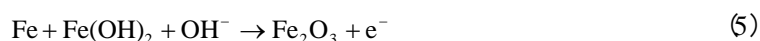
In this case, the density of the corrosion products was enhanced gradually with complete coverage of the surface. It indicated that the Rt values increased with corrosion reaction propagation and reached the maximum at the crevice thickness of 400 μm. The size of the pits on the sample surface decreased, with the reaction transforming from uniform to localized corrosion. When the thickness of crevice increased to δ>400μm, the oxygenation reaction would dominate in the cathode reaction process.Thus, the depolarization was enhanced due to the increasing oxygen content in the crevice

section, along with the enhancement in the iron dissolution reaction [36]. It indicated that the R_t values decreased with the crevice thickness, whereas the corrosion process was aggravated. Meanwhile, the corrosion products mainly contained Fe_2O_3, which had loose structure, thus, providing a little protection of the matrix. The corrosion reaction was observed to be enhanced. The corrosion appeared uniform corrosion and was more severe than the previous segments [37].

4. CONCLUSIONS

(1) X80 steel revealed the passivation of the anodic polarization in the soil simulated solution for the crevice thickness $\delta < 70$ μm. The passivation decreased on increasing the thickness, and the reaction transformed into anodic dissolution.

(2) As the crevice thickness varied in the range 35 μm$< \delta <$150 μm, the corrosive nature of the trapped solution enhanced with H^+ enrichment. The H^+ concentration reached the maximum at the crevice thickness of 150 μm. For the crevice thickness in the range 35 μm$< \delta <$150 μm, the corrosion reaction became strong, with the R_t values increasing with more O_2 diffusing into the solution.

(3) the corrosion products demonstrated a regular slice structure for the low crevice thickness, and a uniform surface corrosion is noted after the removal of the corrosion products. As the crevice thickness reached 150 μm, the substrate surface exhibited the pitting features, with more serious corrosion process. For the crevice thickness more than 600 μm, the corrosion products formed loose chippings, and the corrosion reaction transformed into the uniform corrosion process.

References

1. Y.B. Guo, T. Meng, D. G. Wang, H.Tan and R. Y. He, *Eng. Fail. Anal.*, 78(2017)87.
2. H.X. Wan, D. D. S, Z.Y. Liu, C.W. Du, C. Z. P. Zheng, Z.G. Wang, D. Ding and X. G. Li, *Constr. Build. Mater.*, 154(2017) 580.
3. D. N. Dang, Lanarde. L, Jeannin. M, Sabot. R and Refait. P, *Electrochim. Acta*, 176(2015)1410.
4. F. M. Song, *Corros. Sci.*, 55(2012)107.
5. B. Vuillemin,R. Oltra,R. Cottis and D. Crusset, *Electrochim. Acta*, 52(2007):7570.
6. M. Javidi and S. B. Horeh, *Corros. Sci.*, 80(2014)213.
7. M. C. Yan, J. Q. Wang, E. Han and W. Ke, *Corros. Sci.*, 50(2008)1331.
8. X.Chen, F. J. Gao, Y. L. Wang and C. He, *Mater. Des.*, 89(2016)196.
9. A. Fu and Y. F. Cheng,*Corros. Sci.*, 52(2010)612.
10. M. C. Yan, J. Q. Wang, E.H. Han, C. Sun and W. Ke,*Acta. Metall.Sin.*, 50(2014)1137.
11. F.Varela, M. Y. J.Tan and M. Forsyth, *Electrochim. Acta*, 186(2015)377.
12. 12.M.Latino, F.Varela, M. Tan and M. Forsyth, *Prog. Org. Coat.*, 134(2019)58.
13. G. R. Wang, Y. W. Shao, Y. Q. Wang, G. Z. Meng and B. Liu, *J. Chin. Soc. Corros. Prot.*, 39(2019)235.
14. T. L. Zhao, Z. Y. Liu, X. X. Xu, Y. Li, C. W. Du and X. B. Liu, *Corros. Sci.*, 157(2019)146.

15. M. C. Yan, J. Xu, L. B. Yu and T. Q. Wu, *Corros. Sci.*, 110(2016)23.
16. A.Eslami, R.Kania, B.Worthingham, G. V. Boven, R.Eadie and W. Chen, *Corros. Sci.*, 53(2011)2318.
17. K. Wang, F. B. Varela and M. Y. Tan, *Corros. Sci.*, 150(2019)151.
18. M. T. Majd, T.Shahrabi and B.Ramezanzadeh, *Appl. Surf. Sci.*, 464(2019)516.
19. Z. Y. Liu, W. R. Zheng, L. W. Wang, Z. Cui and X. G. Li, *J. Univ. Sci. Technol. B.*, 36(2014)1483.
20. A. H. J. Mofidabadi, G. Bahlakeh and B.Ramezanzadeh,,*J. Mol. Liq.*, 314(2020)113658.
21. A. Fu and Y. F. Cheng, *Corros. Sci.*, 51(2009)914.
22. W. Wu, Z.Y. Liu, X.G. Li and C. W. Du, *J.Electroanal. Chem.*, 845(2019)92.
23. A. Eslami,R. Kania,B. Worthingham,G. V. Boven,R. Eadie andW. Chen, *Corros. Sci.*, 53(2011)2318.
24. X. Chen,X. G. Li,C. W. Du andP. Liang, *Int. J. Min. Met. Mater.*,16(2009)525.
25. H. C. Ma, B. Zhao, Z. Y. Liu and C. W. Du, *Conster. Build. Mater.*, 243(2020)118203.
26. X. Chen,X. G. Li,C. W. Du andY.F. Cheng, *Corros. Sci.*, 51(2009)2242.
27. A. Fu and Y. F. Cheng, *Corros. Sci.*, 52(2010)2511.
28. F. M. Song and N.Sridhar, *Corros. Sci.*, 50(2008)70.
29. H.Liu and Y. F. Cheng, *Corros. Sci.*, 133(2018)178.
30. H.Liu and Y. F.Cheng, *Electrochim. Acta*, 253(2017)368.
31. X. Chen, G. F. Wang, F. J. Gao, Y. L. Wang and C. He, *Corros. Sci.*, 101(2015)1.
32. T. Q. Wu, M. C.Yan, L. B. Yu, H. T.Zhao, C. Sun, F. C. Yin and W. Ke, *Corros. Sci.*, 157(2019)518.
33. F. Gan, Z. W. Sun and G. Sabde, *Corrosion*, 50(1994)804.
34. Y. F. Cheng and L. Niu, *Electrochem. Commun.*, 4(2007)9.
35. Z. Y. Liu, X. G. Liand Y. F. Cheng, *Corros. Sci.*, 55(2012)55.
36. Z. S. Li, Z. Y. Liu, C. W. Du and C, Y. Li, *Surf. Technol.*, 7(2016)45.
37. B. Zhao, C. W. Du, Z. Y. Liu, X. G. Li, J. K. Yang and Y. Q. Li,*Acta. Metall. Sin*., 12(2012)48.